RSC Advances

PAPER

View Article Online
View Journal | View Issue

Cite this: *RSC Adv.*, 2025, **15**, 28492

Desymmetrization on electron-withdrawing groups in single benzene fluorophores for fine tuning of photophysical properties and applications

Jun Yeong Kim,†[a] Haein Kim,†[a] EunHo Hong,†[a] Dopil Kim,[a] Chae Young Ryu,[a] Dokyoung Kim,[b] JunWoo Kim,*[a] Myung Hwan Park*[c] and Min Kim*[a]

In this study, a series of unsymmetrical single-benzene fluorophore (SBF) derivatives were systematically synthesized by selectively disrupting the ester symmetry of standard diamino terephthalate-type analogs *via* alternative synthetic routes. Various electron-donating groups (EDGs) and electron-withdrawing groups (EWGs) were introduced at one ester group position, yielding 12 **A** series compounds with emission wavelengths spanning from 440 to 578 nm. EDGs led to blue-shifts, while EWGs induced red-shifts relative to the symmetric parent compound. This trend can be attributed to electronic modulation of frontier molecular orbitals. Density functional theory (DFT) calculations confirmed that increasing EWG strength led to a gradual reduction in the HOMO–LUMO energy gap, in agreement with experimental emission trends. Although substituent effects were evident, the overall spectral shifts between symmetric and unsymmetric structures remained modest, indicating structural robustness of the core scaffold. In addition, a series of monoamino **B** series compounds (12 analogs) were prepared to examine the photophysical consequences of removing one amino group. These consistently showed blue-shifted emissions compared to the **A** series, attributed to reduced conjugation and secondary hydrogen bonding. Finally, ester hydrolysis of selected compounds generated **C** series carboxylic acids, enabling pH-dependent fluorescence switching. Notably, **C-COMe** exhibited multicolor emission—from blue to orange—across varying pH conditions. These results demonstrate a modular strategy for tuning emission behavior in SBFs through controlled symmetry and functionalization.

Received 23rd May 2025
Accepted 3rd August 2025

DOI: 10.1039/d5ra03628c

rsc.li/rsc-advances

Introduction

The development of simple organic fluorophores is an emerging area of research, driven by the increasing demand for efficient materials in display technologies. Among these, single benzene fluorophores (SBFs) have garnered significant attention due to their low molecular weights, compact structures, and tunable optical properties, offering a minimalist approach compared to traditional organic light-emitting diode (OLED) materials.[1–8] Recent studies have extensively explored the photophysical properties of SBFs, which are influenced by the incorporation of electron-donating groups (EDGs) and electron-withdrawing groups (EWGs) into a single benzene backbone, forming push–pull systems that enable precise emission control.[9–16]

In most SBF designs, two symmetrical functional group conformations are predominantly used, with two EDGs and two EWGs arranged oppositely on the benzene backbone.[17–22] For example, terephthalic acid and terephthaldehyde, featuring two carboxylic acid or aldehyde groups in *para*-configurations, respectively, serve as common cores for EWGs, while EDGs such as amino or hydroxyl groups are introduced to control emission properties.[23–31] Various combinations of EDGs and EWGs have been systematically studied, revealing a strong correlation between the electronic nature of the substituents and the emission wavelength.[32–39] Recent reviews have summarized these findings, highlighting the growing understanding of the relationship between molecular structure and photophysical behavior.[40,41]

More recently, we have focused on positional control of functional groups in SBFs to achieve refined tuning of their optical properties. For instance, the use of *para*-configured amino groups as EDGs and ester groups as EWGs has demonstrated the critical role of symmetrical arrangements in

[a]*Department of Chemistry, Chungbuk National University, Cheongju, 28644, Republic of Korea. E-mail: jwkim0@chungbuk.ac.kr; mikim@chungbuk.ac.kr*

[b]*Department of Biomedical Science, Graduate School, Kyung Hee University, Seoul, 02447, Republic of Korea*

[c]*Department of Chemistry Education, Chungbuk National University, Cheongju, 28644, Republic of Korea. E-mail: mhpark98@chungbuk.ac.kr*

† J. Y. Kim, H. Kim, and E. Hong equally contributed to this work.

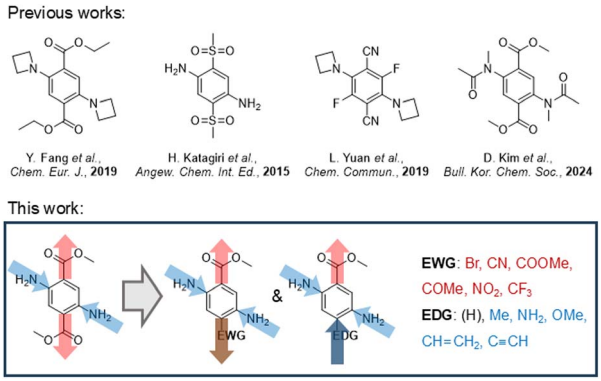

Fig. 1 Desymmetrization of diamino- and diester-SBFs with various functional groups.

enhancing fluorescence efficiency.[42–44] In 2,5-diamino terephthalate derivatives, subtle modifications to the amino groups revealed the importance of symmetrical functionalization in achieving consistent emission characteristics, as well as the potential for detailed wavelength adjustments through structural variations.[45–48]

Building on our interests in advancing the photophysical properties of SBFs, we explored desymmetrization strategies, such as altering EWGs or introducing unsymmetrical substituents. This shift away from traditional symmetric architectures offers new opportunities to fine-tune emission wavelengths, quantum yields, and environmental responsiveness (Fig. 1). Herein, we report a series of desymmetrized SBF derivatives (12 diamino **A** series and 12 monoamino **B** series) and their detailed photophysical properties. Interestingly, **A** series exhibited multicolor emission in the range from blue (440 nm) to red (578 nm) depending on the substituents. Furthermore, the quantum yields of diamino **A** series compounds were found to be higher than those of monoamino **B** series compounds. Notably, carboxylated-appended **C** series (**C-COMe** and **C-CN**) showed pH-responsive fluorescent change. The theoretical calculations supported the experimental results.

Results and discussion

Desymmetrization of EWG and their photophysical properties

The substitution of one of the ester groups from dimethyl 2,5-diaminoterephthalate has been mainly investigated with a diverse range of functional groups (Fig. 1). Six representative EWGs including acetyl, bromo, cyano, ester, nitro, and trifluoromethyl were selected for substitution at the ester position. The electronic configurations in SBFs have been altered by EWG substitutions. In addition, EDGs could be installed instead of one ester during this synthetic approaches. In this case, the obtained molecules have three EDGs and one EWG, which is not a typical structural motif for SBFs. Therefore, the effect of push–pull system could be investigated with the substitution of EWG to EDG. Five EDGs such as amino, vinyl, ethynyl, methoxy, and methyl were designed, and the ester removed (*i.e.*, substitution of ester to H) was also prepared as a standard molecule between EDGs and EWGs. This design deviates from typical SBF systems, which generally rely on symmetric configurations of two identical EDGs or EWGs. By intentionally introducing asymmetry through selective substitution, we aimed to modulate the internal charge distribution and explore push–pull effects on emission properties. Such a strategy provides insight into how electronic asymmetry, especially from mixed donor–acceptor combinations, influences the HOMO–LUMO gap and fluorescence behavior.

Although the conjugation, steric effect and stereoconformation, and interactions between functional groups should be considered, the simple, electronic characters of all substituents were firstly evaluated with the Hammett constants before synthesis (Table S1 in SI). In the present SBF system, substituents are introduced at the *para*-position of the ester group, the *meta*-position of the first amine group, and the *ortho*-position of the second amine group. Since standard Hammett constants are only defined for *para*- and *meta*- positions,[49,50] we considered only the substituents at these two positions for electronic correlation. The *ortho*-substituted second amine was excluded from this analysis, as its electronic effects are complicated by steric and possible hydrogen-bonding interactions, and no standard σ values are available for this position.

In general, two-step nitration and reduction were performed to introduce NH_2 group on the methyl benzoate with the desired functional groups (amino, bromo, methoxy, methyl, and trifluoromethyl). In addition, this nitration–reduction was successfully incorporated with symmetrical diester molecules and unsubstituted monoester (Fig. 2a). The nitration was performed with *N*-acetylated compound, and the reduction of nitro group was carried out under H_2–Pd/C condition. As a result, EDG-substituted **A-NH$_2$**, **A-OMe**, and **A-Me** along with EWG-

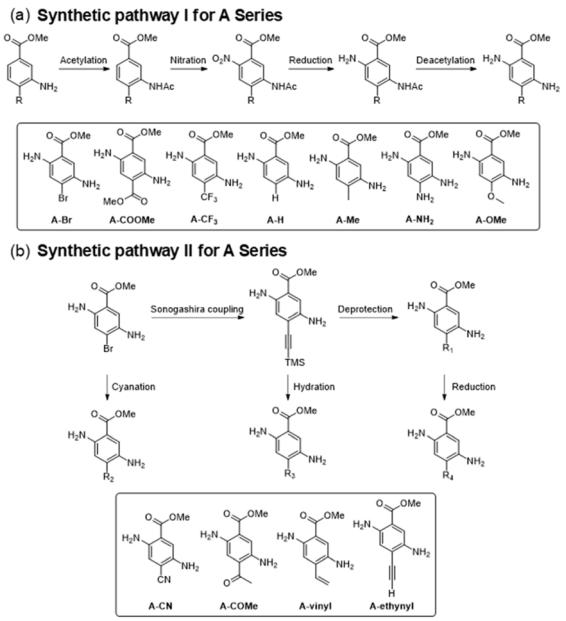

Fig. 2 Synthetic pathways to EWG-desymmetrized SBF series **A**; (a) scheme for **A-Br**, **A-COOMe**, **A-CF$_3$**, **A-H**, **A-Me**, **A-NH$_2$**, and **A-OMe**. (b) Scheme for **A-CN**, **A-COMe**, **A-vinyl**, and **A-ethynyl**.

substituted **A-Br** and **A-CF_3** were prepared through this general pathway (Fig. 2a). **A-NO_2** was prepared by alternative method for **A-NH_2** preparation. Then, Br-functionalized **A-Br** was utilized as a starting material to prepare new derivatives. Nitrile-containing **A-CN** was synthesized through direct Cu-catalyzed cyanation of **A-Br**. In addition, the Sonogashira cross-coupling to install TMS-acetylide (TMS = trimethylsilyl) was performed and this intermediate was successfully converted to **A-ethynyl** through TMS deprotection. Acetyl-functionalized **A-COMe** was obtained through hydration of alkyne in **A-ethynyl**. Finally, alkene-functionalized **A-vinyl** was achieved through selective hydrogenation of alkyne (Fig. 2b). The structures of the obtained **A** series were confirmed by ^{1}H and ^{13}C NMR (Nuclear Magnetic Resonance) and mass spectrometry (see SI for detail). For certain derivatives such as **A-CN** and **A-ethynyl**, low overall yields (1–3%) were observed, largely due to multi-step synthesis and challenging purification. Instability of intermediates and side reactions during cyanation and deprotection steps also contributed to these outcomes.

Next, the photophysical properties of the **A** series were investigated, including excitation, emission, Stokes shift, quantum yield, lifetime, full width at half maximum (FWHM), and absorption from UV-vis spectra (Table 1 and Fig. S1–S10). The excitation wavelength (λ_{ex}) for each compound was determined as the wavelength that gave the maximum emission intensity during excitation scans. The absorption bands can be assigned to π–π* transition centered on the benzene core, and their maximum absorption wavelengths (λ_{abs}) were red- or blue-shifts depending on the substituents (Fig. S1–S10). For emission, all SBFs cover a wide range of fluorescence emission wavelengths, from the blue region to the red region in general (from 440 nm to 578 nm, Fig. 3a). A direct correlation was observed between the electronic nature of the substituent and the emission wavelength. Generally, EDGs such as methoxy and amino caused blue-shifted emissions, while EWGs such as nitro and ester induced significant red-shifts. As a reference, non-functionalized **A-H** has fluorescence emission at 465 nm, and methoxy (**A-OMe**), amino (**A-NH_2**), and methyl (**A-Me**) groups caused blue-shifted emissions in the range of 440–455 nm (Table 1 and Fig. S2–S5). On the other hand, it was confirmed that EWGs or functional groups with a longer conjugation band have red-shifted emission from the reference. **A-COOMe**, **A-CF_3**, **A-CN**, **A-COMe**, **A-ethynyl**, and **A-vinyl** displayed their emission in the range of 479–578 nm (Table 1, Fig. S1 and S6–S10). To further examine the solvent-dependent photophysical behavior, the emission spectra of selected compounds (**A-OMe**, **A-COMe**, and **A-ethynyl**) were additionally measured in polar solvents such as tetrahydrofuran (THF) and acetonitrile (MeCN). Compared to toluene, moderate red-shifts of up to ~20 nm were observed, suggesting the presence of weak charge transfer (CT)

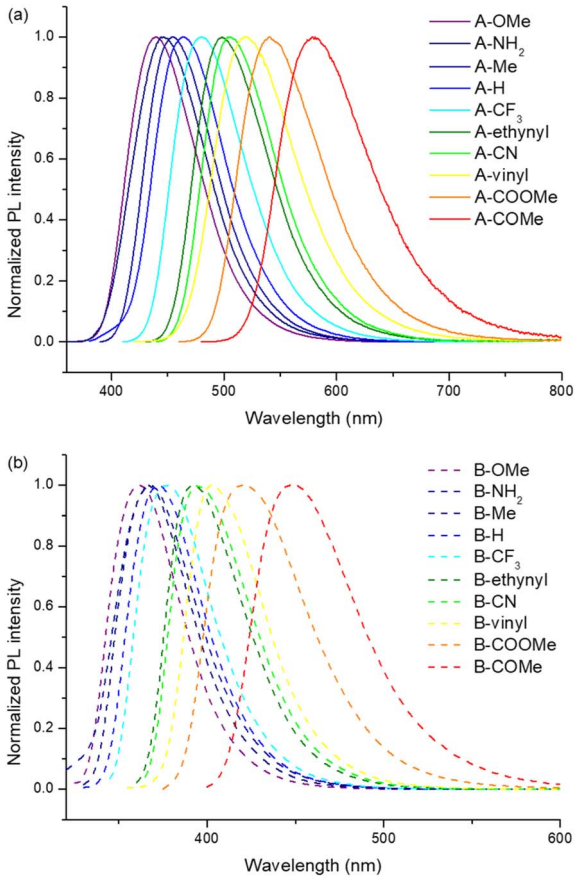

Fig. 3 Emission spectra of (a) A series compounds (solid lines), (b) B series compounds (dashed lines) in toluene solution at 298 K (20 μM).

Table 1 Summarized photophysical properties of the A series in degassed toluene (20 μM) at 298 K

Compound	λ_{abs} [nm] (ε ×10^3 M^{-1} cm^{-1})	λ_{ex} [nm]	λ_{em} [nm]	Stokes shift [cm^{-1}]	φ_{PL} [a] [%]	τ [b] [ns]	FWHM [nm]	k_r [×10^7 s^{-1}]	k_{nr} [×10^8 s^{-1}]
A-COOMe	443 (3.91)	443	539	4020	53	11.36	84	4.7	0.4
A-H	375 (1.94)	376	465	5090	47	9.51	71	5.0	0.6
A-OMe	356 (8.51)	358	440	5206	49	7.51	75	6.5	0.7
A-NH_2	345 (4.99)	346	446	6480	88	7.74	71	11.4	0.1
A-Me	372 (2.99)	370	455	5049	39	8.57	74	4.6	0.7
A-CF_3	390 (2.32)	394	479	4504	51	10.8	74	4.7	0.5
A-ethynyl	414 (4.11)	414	497	4034	61	9.90	76	6.1	0.4
A-CN	425 (3.30)	423	504	3799	78	11.23	75	6.9	0.2
A-vinyl	405 (5.81)	406	517	5288	45	9.81	85	4.6	0.6
A-COMe	466 (4.62)	465	578	4204	13	5.32	91	2.4	1.6

[a] Absolute photoluminescence quantum yield (PLQY). [b] Emission lifetime.

character in these systems (Table S2, and Fig. S11–13). In addition, to evaluate the contribution of conformational flexibility to the Stokes shift, emission spectra were recorded in a rigid matrix at 77 K. However, no significant spectral changes were observed compared to the room temperature data, indicating that geometric reorganization in the excited state is not a dominant factor (Table S3, and Fig. S14–S16). Thus, the observed Stokes shifts are mainly attributed to weak CT behavior, as supported by solvatochromic trends.

As a counterpart, the standard symmetrical **A-COOMe** and the unsymmetrical **A-COMe** were carefully compared, as they possess similar electronic characteristics (*i.e.*, Hammett constants of 0.45 and 0.50, respectively), the ability to form hydrogen bonds with the *ortho*-amino group, comparable conjugation lengths, and closely related molecular structures. As a result, all photophysical properties—except quantum yield—were found to be quite similar. In particular, both emission and absorption wavelengths showed only minor differences between the symmetrical ester and the unsymmetrical ketone. Therefore, the use of symmetrical EWG-based conformations in new SBF design and synthesis can be flexibly adapted depending on the situation. In addition, it was clearly demonstrated that the presence of two EWGs is not essential for constructing functional SBFs; combinations of a single EWG with three EDGs also offer viable pathways for designing new SBF molecules. For the quantum yield, all the obtained **A** series demonstrated good absolute quantum efficiencies, ranging from 13% to 88% in 20 μM toluene solution condition (Table 1).

Synthesis and photophysical properties of monoamino SBFs and comparisons

Additional desymmetrization on electron-donating groups (EDGs, such as two amino groups) was achieved through the established synthetic pathways. The monoamino-type SBFs (**B** series) were successfully synthesized by omitting the nitration–reduction steps shown in Fig. 2 (also referenced as Fig. S17). A total of 12 **B** series SBFs, each containing one ester group and one amino group in a *meta*-relationship, were prepared. These compounds also bear an additional functional group—either an EDG or an EWG—at the *para*-position relative to the ester. Two core structures, **B-COOMe** (lacking one amino group compared to **A-COOMe**) and **B-H**, are commercially available, while the bromo-functionalized **B-Br** serves as a key intermediate for the synthesis of other **B** series derivatives (Fig. S17).

The photophysical properties of the **B** series were measured and generally exhibited trends similar to those observed in the **A** series (Table 2 and Fig. S18–S27). Substitution with EDGs at the *para*-position of the ester group (*e.g.*, **B-OMe**, **B-NH$_2$**, and **B-Me**) resulted in blue-shifted emissions ranging from 362 to 368 nm, compared to the non-functionalized **B-H** (373 nm). Conversely, substitution with EWGs or groups featuring extended π-conjugation (*e.g.*, **B-CF$_3$**, **B-CN**, **B-COOMe**, **B-COMe**, **B-ethynyl**, and **B-vinyl**) led to red-shifted emissions ranging from 377 to 448 nm.

Notably, across all substituent types—both EDGs and EWGs—the **B** series consistently showed shorter emission wavelengths than the corresponding **A** series under desymmetrized EWG conditions (Fig. S18–S27). EWG substitution on the ester group (*e.g.*, CF_3, CN, COOMe, and COMe) resulted in a 102–130 nm blue shift when comparing the **A** and **B** series. In contrast, EDG substitution (*e.g.*, OMe, NH_2, and Me) led to a smaller blue shift of 78–90 nm between the two series (Tables 1 and 2). It is well established that diamino-based SBFs exhibit longer emission wavelengths than their monoamino counterparts.[51] This red-shift is primarily attributed to the enhanced electron-donating effect of the second amino group and the formation of intramolecular hydrogen bonding. The additional amino group increases the electron density of the conjugated system, while the intramolecular hydrogen bond between the *ortho*-positioned ester and amino group helps to rigidify the structure, promoting greater electronic delocalization. As a result, the highest occupied molecular orbital (HOMO)-lowest unoccupied molecular orbital (LUMO) energy gap is reduced, leading to red-shifted emission. In contrast, monoamino derivatives (**B** series) lack both the additional EDG and secondary hydrogen-bonding interactions, resulting in reduced delocalization and, consequently, blue-shifted emission. In terms of quantum yield, the **B** series exhibited moderate absolute quantum efficiencies, which were generally lower than those of the **A** series under toluene conditions (ranging from 20% to 64%, Table 2).

Table 2 Summarized photophysical properties of the B series in degassed toluene (20 μM) at 298 K

Compound	λ_{abs} [nm] ($\varepsilon \times 10^3$ M^{-1} cm^{-1})	λ_{ex} [nm]	λ_{em} [nm]	Stokes shift [cm^{-1}]	φ_{PL}[a] [%]	τ[b] [ns]	FWHM [nm]	k_r [$\times 10^7$ s^{-1}]	k_{nr} [$\times 10^8$ s^{-1}]
B-COOMe	366 (7.00)	363	420	3739	64	10.19	63	6.3	0.4
B-H	321 (4.23)	321	373	4343	31	0.54	47	57.5	12.8
B-OMe	314 (7.67)	314	362	4223	21	0.59	48	35.0	13.5
B-NH$_2$	308 (18.19)	313	368	4775	28	0.62	49	44.7	11.7
B-Me	316 (3.82)	315	365	4349	20	0.64	54	31.7	12.5
B-CF$_3$	325 (8.28)	329	377	3870	28	0.58	51	48.8	12.4
B-ethynyl	347 (6.07)	345	392	3475	54	5.71	52	9.5	0.8
B-CN	349 (5.24)	350	396	3319	52	8.27	54	6.3	0.6
B-vinyl	337 (6.07)	342	404	4487	41	4.99	50	8.2	1.2
B-COMe	385 (5.18)	385	448	3653	23	3.60	67	6.3	2.2

[a] Absolute photoluminescence quantum yield (PLQY). [b] Emission lifetime.

In addition, the photophysical properties of bromo- and nitro-functionalized SBFs are particularly noteworthy. Both diamino- and monoamino- desymmetrized SBFs containing bromo- and nitro- substituents (**A-Br**, **A-NO$_2$**, **B-Br**, and **B-NO$_2$**) exhibited fluorescence quenching. The heavy atom effect of the bromo group led to significantly reduced quantum yields in both **A-Br** and **B-Br**.[52] Meanwhile, the strong electron-accepting nature of the nitro group disrupted radiative decay pathways.[53,54] Interestingly, **A-Br** exhibited fluorescence at 77 K, which is likely due to the suppression of non-radiative decay through restricted molecular motion in the rigidified environment (Fig. S28).[52–54] In contrast, **B-Br** showed no emission even at 77 K. To further investigate this behavior, time-resolved fluorescence measurements were conducted, and emission spectra were recorded at 77 K for **A-Br** (Table S4). However, no phosphorescence was observed under these conditions, suggesting that intersystem crossing (ISC), if occurring, does not result in efficient triplet-state emission. This implies that while the Br atom may promote ISC, non-radiative decay pathways are likely dominant in this system.

Computational studies for desymmetrization on SBFs

Density functional theory (DFT) calculations were conducted to understand the electronic structures of SBF molecules, particularly focusing on the effects of desymmetrization involving EWGs (ester). All calculations were performed using the GAUSSIAN09 software package with the CAM-B3LYP functional and the 6-31G basis set.[55] Solvent effects were accounted for using the conductor-like polarizable continuum model (CPCM), with toluene as the chosen solvent to match the experimental conditions. To systematically evaluate the influence of different substituents, three representative SBF compounds were selected: **A-OMe** (representing an EDG), **A-ethynyl** (illustrating extended π-conjugation), and **A-COMe** (representing an EWG). These substrates were chosen to independently assess the electronic effects associated with desymmetrization through electron donation, conjugation, and withdrawal.

The calculation results exhibited a clear trend in the HOMO–LUMO energy gap, which progressively decreased in the order of **A-OMe** > **A-ethynyl** > **A-COMe** (Fig. 4a). This trend is in excellent agreement with experimental emission data, where a red-shift in fluorescence was observed as the electronic character of the substituents changed from donor to acceptor. Specifically, **A-OMe** exhibited an emission peak at 440 nm, followed by **A-ethynyl** at 497 nm, and **A-COMe** at 578 nm, corresponding directly with the narrowing of the calculated HOMO–LUMO energy gaps. Notably, **A-COMe** exhibited a pronounced reduction in transition energy, which can be attributed to its dual functionality: the carbonyl group acts both as an electron-withdrawing substituent and as a hydrogen-bonding partner with the *ortho*-amino group. This interaction further stabilizes the LUMO level and enhances orbital polarization, leading to the observed red-shift in emission. The reduction of transition energy is strongly related to the electron-donating strength of the groups modulated by the variable substituent. It can be observed that electron density is transferred from the amino groups to the

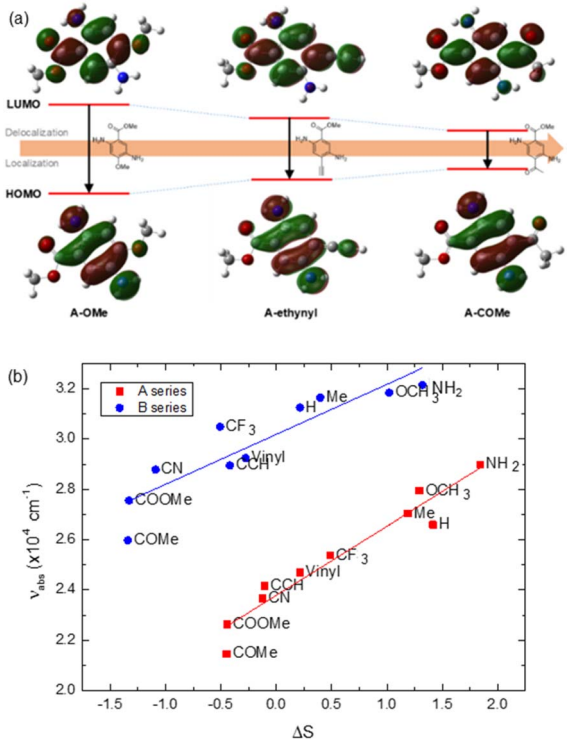

Fig. 4 (a) HOMO–LUMO structures and energy levels of desymmetrized SBFs; **A-OMe**, **A-ethynyl**, and **A-COMe**. (b) Correlation between localization parameter and the absorption transition energy for **A** series (red) and **B** series (blue) compounds.

carbonyl in ester, and the common substituents in **A**-type desymmetrized SBFs (Fig. S29). In **A-OMe**, both the amino and methoxy groups act as electron donors, leading to localization of electron density on the central benzene ring upon electronic excitation. On the other hand, in **A-COMe**, the acetyl group withdraws electron density from the donor groups upon excitation, resulting in a LUMO with significantly more delocalized electronic density compared to the other SBFs (Fig. 4a).

Conversely, as the electron-withdrawing strength of the substituent increases, the electron density on the carbonyl group of ester in the HOMO decreases, leading to stronger localization of charge on the central SBF core. As the LUMO becomes more delocalized while the HOMO becomes more localized, the overlap between the two molecular orbitals diminishes. As understood from simple quantum models such as the particle-in-a-box, delocalized eigenstates generally correspond to lower energy levels, whereas localized states are associated with higher energies. Therefore, this computational result clearly illustrates how the electron-donating or -withdrawing strength of the substituent influences the transition energy. Similar trends were also observed from the DFT calculation on **B-OMe**, **B-ethynyl**, and **B-COMe** for HOMO–LUMO energy gap and energy transition (Fig. S30 and S31).

We further evaluated the spatial characteristics of the frontier orbitals by introducing a localization parameter, $\Delta S = \Sigma_{\mathrm{LUMO}}{}^2 - \Sigma_{\mathrm{HOMO}}{}^2$, derived from the statistical variance ($\Sigma_{\mathrm{MO}}{}^2$) of the orbital coefficient across atoms. A smaller ΔS value suggests that the

LUMO is more delocalized across the molecular framework. The relationship between ΔS and the transition frequency for both A and B series shows a consistent trend (Fig. 4b). This correlation suggests that substituent-dependent changes in electron delocalizability influence the transition frequencies across both **A** and **B** series. In addition, a negative relationship is observed between the Hammett constant (σ_{Hammett}) of the substituents and the localization parameter ΔS, as shown in Fig. S32, indicating that EWG tend to promote orbital delocalization. These results underscore the role of ΔS as a complementary descriptor to the HOMO–LUMO gap and demonstrate how substituent electronic effects influence both the energy and spatial distribution of excited states in desymmetrized SBF systems.

The S_0–S_1 transition in all cases was found to be predominantly of π–π* character, with no meaningful contribution from nonbonding orbitals, ruling out n–π* transitions. To evaluate the CT character, we calculated the electronic dipole moment difference between the HOMO and LUMO ($\Delta\mu$) in Debye. While $\Delta\mu$ and transition energy appear to show a positive correlation (Fig. S33a and b), this trend is likely a consequence of the positive correlation between $\Delta\mu$ and ΔS (Fig. S33c and d), rather than direct evidence that CT character affects the transition frequency. CT character typically influences transition energy in systems where solvation plays a significant role. However, since $\Delta\mu$ shows little correlation with the Stokes shift in our data (Fig. S33e and f), it is more reasonable to attribute the variation in transition frequency to differences in electron delocalizability, as discussed above.

Carboxylic acid-derivatives as pH-responsive SBFs

SBFs represent a promising platform for the development of pH-responsive fluorescent molecules due to their simple molecular structures and good solubility. The pH sensitivity of SBFs is particularly valuable for applications in sensing and bioimaging.[56–59] In addition to the inherent basicity of the amino groups in these SBFs, acidic functionality can be introduced through hydrolysis of the ester moiety to the corresponding carboxylic acid (Fig. S34). Accordingly, hydrolysis of the **A** series compounds was carried out to produce a new set of carboxylic acid-containing compounds, designated as the **C** series. Among them, two representative derivatives; **C-CN** and **C-COMe**, were selected for further study due to their efficient synthesis and pronounced color-changing properties. These compounds were primarily investigated for their pH-dependent optical behavior across a pH range of 1 to 13 in a THF/PBS (pH 7.4) mixed solvent system (Fig. 5).

In general, **C-CN** exhibited yellow-green fluorescence, with a gradual color shift toward green as the pH increased. This change is mainly attributed to the deprotonation of the carboxylic acid to its corresponding carboxylate anion. In contrast, **C-COMe** showed a wider range of color variation, with fluorescence spanning from blue to green, yellow, and orange depending on the pH conditions (Fig. 5). To support the interpretation of pH-dependent optical properties, the pK_a values of the carboxylic acid moieties in **C-CN** and **C-COMe** were determined through acid–base titrations (Table S5 and Fig. S35 and S36, pK_a = 2.93 and 2.84, respectively). Based on these values, UV-vis and PL spectra were recorded at pH 3, 5, 7, and 10, providing a more comprehensive picture of their pH-responsive behavior (Table S6 and Fig. S37–46).

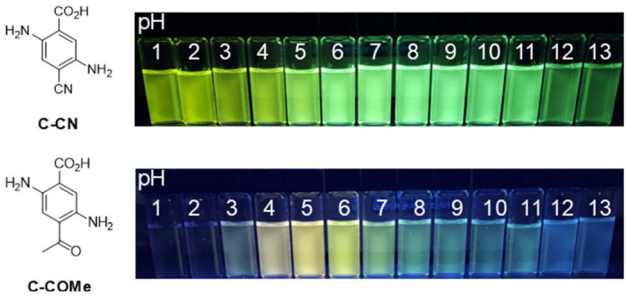

Fig. 5 Optical images of **C-CN** and **C-COMe** under various pH solution and UV irradiation.

This diversity is believed to arise from structural changes associated with intramolecular hydrogen bonding. Specifically, **C-COMe** can form two types of hydrogen bonds—between the amino and carboxylic acid groups, and between the amino and ketone groups—contributing to its pH-responsive optical behavior (Fig. 5). To further understand the origin of the pH-dependent emission shifts, TD-DFT calculations were conducted on the protonated and deprotonated forms of **C-CN** and **C-COMe**. While the computed trends generally support the experimental observations for **C-COMe**, discrepancies in the case of **C-CN** suggest that specific solvation effects may also influence the excited-state properties. The incorporation of desymmetrized EWGs in the SBF framework successfully enabled the introduction of carboxylic acid functionalities for pH-responsive systems, while also providing fine tunability of their photophysical properties.

Conclusions

This study presents a systematic approach to the desymmetrization of diamino terephthalate-type SBFs through selective substitution of one ester group with various electron-donating and electron-withdrawing functionalities. Twelve unsymmetrically substituted SBF derivatives (**A** series) were synthesized and fully characterized in terms of their photophysical properties. The emission wavelengths spanned a broad range (440–578 nm), and substituent-dependent shifts were clearly observed: EDGs induced blue-shifted emission, while EWGs caused red-shifts relative to the symmetric reference compound. Despite the introduction of asymmetry, the core scaffold retained a high degree of spectral and structural integrity, indicating its robustness for further functionalization.

In parallel, monoamino-type analogs (**B** series) were prepared to evaluate the electronic consequences of removing one amino group. Across all substituent types, the **B** series consistently exhibited shorter emission wavelengths compared to their **A** series counterparts. This emission shift is attributed to reduced conjugation and the absence of intramolecular hydrogen bonding, both of which limit electronic

delocalization. DFT calculations further supported these observations, revealing that the nature of the substituent systematically influences the HOMO–LUMO energy gap in a manner consistent with the experimental trends.

Hydrolysis of selected **A** series compounds afforded the **C** series, incorporating carboxylic acid groups that enable pH-responsive emission and demonstrate how single-site modification can introduce tunable environmental sensitivity. Taken together, this work demonstrates how targeted desymmetrization can be used to rationally modulate photophysical behavior in compact organic fluorophores. Beyond empirical trends, the observed link between structural asymmetry, excited-state properties, and environmental responsiveness offers a design framework for next-generation luminescent materials. The multicolor, pH-sensitive emission profiles of the **C** series suggest particular utility in stimuli-responsive sensing and imaging systems, where spectral tunability and molecular compactness are both highly valued.

Author contributions

Jun Yeong Kim: writing – original draft, methodology, investigation, data curation. Haein Kim: visualization, formal analysis, data curation. Eunho Hong: investigation, data curation, visualization. Dopil Kim: methodology, investigation. Chae Young Ryu: methodology, investigation, data curation. Dokyoung Kim: conceptualization, formal analysis. JunWoo Kim: supervision, investigation, funding acquisition. Myung Hwan Park: supervision, formal analysis, data curation. Min Kim: conceptualization, writing – original draft, visualization, supervision, funding acquisition.

Conflicts of interest

There are no conflicts to declare.

Data availability

The data supporting this article have been included as part of the SI. See DOI: **https://doi.org/10.1039/d5ra03628c**.

Acknowledgements

This work was supported by the National Research Foundation of Korea (NRF), funded by the Ministry of Science and ICT (RS-2024-00352112 for M. K.; RS-2023-00210065 for J.W. K.). Dr Dopil Kim was financially supported by the NRF funded by the Ministry of Education (PhD student research fellowship, RS-2023-00274850).

Notes and references

1 A. Huber, L. Schmidt, T. Gatz, J. Bublitz, T. Rex, S. T. N. Sailaja, E. Verheggen, L. Höfmann, C. Wolper, C. A. Strassert, S. K. Knauer and J. Voskuhl, *Chem.–Eur. J.*, 2025, **31**, e202404263.
2 S. Ghosh, S. Kumar, S. Suneesh, H. Bhambri, S. K. Mandal, S. Ghosh, R. Chowdhury and P. S. Addy, *J. Org. Chem.*, 2024, **89**, 9303–9312.
3 X. Zhang, J. Wang, F. Yu, X. Huang, N. Wang, T. Wang and H. Hao, *Cryst. Growth Des.*, 2022, **22**, 3198–3205.
4 J. Kim, J. M. An, Y. Jung, N. H. Kim, Y. Kim and D. Kim, *Nanomaterials*, 2021, **11**, 2036.
5 Y. Fan, J. Ma, H. Liu and T. Liu, *Molecules*, 2022, **27**, 5522.
6 T. Raghava and S. Banerjee, *Chem.–Asian J.*, 2024, **19**, e202400898.
7 B. Tang, H. Liu, F. Li, Y. Wang and H. Zhang, *Chem. Commun.*, 2016, **52**, 6577–6580.
8 M. Shimizu, Y. Takeda, M. Higashi and T. Hiyama, *Angew. Chem., Int. Ed.*, 2009, **48**, 3653–3656.
9 Z. Wang, G. Horiguchi, H. Kamiya and Y. Okada, *Chem.–Eur. J.*, 2023, **29**, e202301411.
10 L. Yuan, W. Lin, K. Zheng and S. Zhu, *Acc. Chem. Res.*, 2013, **46**, 1462–1473.
11 Y. Okada, M. Sugai and K. Chiba, *J. Org. Chem.*, 2016, **81**, 10922–10929.
12 A. M. Thooft, K. Cassaidy and B. VanVeller, *J. Org. Chem.*, 2017, **82**, 8842–8847.
13 M. S. Tsai, C. L. Ou, C. J. Tsai, Y. C. Huang, Y. C. Cheng, S. S. Sun and J. S. Yang, *J. Org. Chem.*, 2017, **82**, 8031–8039.
14 F. Ogawa, Y. Karuo, R. Yamazawa, K. Miyanaga, K. Hori, K. Tani, K. Yamada, Y. Saito, K. Funabiki, A. Tarui, K. Sato, K. Ito, K. Kawai and M. Omote, *J. Org. Chem.*, 2020, **85**, 1253–1258.
15 T. Chatterjee, M. Mandal, S. Mardanya, M. Singh, A. Saha, S. Ghosh and P. K. Mandal, *Chem. Commun.*, 2023, **59**, 14370–14386.
16 S. Sarkar, A. Shil, Y. W. Jun, Y. J. Yang, W. Choi, S. Singha and K. H. Ahn, *Adv. Funct. Mater.*, 2023, **33**, 2304507.
17 J. Christoffers, *Eur. J. Org Chem.*, 2018, **2018**, 2366–2377.
18 N. Wache, C. Schroder, K. W. Koch and J. Christoffers, *ChemBioChem*, 2012, **13**, 993–998.
19 D. Pletsch, F. da Silveira Santos, F. S. Rodembusch, V. Stefani and L. F. Campo, *New J. Chem.*, 2012, **36**, 2506–2513.
20 R. Huang, B. Liu, C. Wang, Y. Wang and H. Zhang, *J. Phys. Chem. C*, 2018, **122**, 10510–10518.
21 X. Zhang, J. Wang, Y. Liu, Y. Hao, F. Yu, D. Li, X. Huang, L. Yu, T. Wang and H. Hao, *J. Phys. Chem. C*, 2021, **125**, 6189–6199.
22 T. Beppu, K. Tomiguchi, A. Masuhara, Y. J. Pu and H. Katagiri, *Angew. Chem., Int. Ed.*, 2015, **54**, 7332–7335.
23 J. Dai, X. Wang, Z. Zhan, C. Wei, Y. Chai, J. Hua, H. Dong, G. Wang, J. Wang, J. Liu and L. Fang, *J. Mater. Chem. C*, 2025, **13**, 9667–9672.
24 Y. Jung, J. H. Jin, Y. Kim, J. H. Oh, H. Moon, H. Jeong, J. Kim, Y. K. Park, Y. Oh, S. Park and D. Kim, *Org. Biomol. Chem.*, 2022, **20**, 5423–5433.
25 B. Tang, M. Li, X. Yu and H. Zhang, *J. Mater. Chem. C*, 2022, **10**, 3894–3900.
26 X. Zhang, J. Wang, F. Yu, X. Cheng, Y. Hao, Y. Liu, X. Huang, T. Wang and H. Hao, *CrystEngComm*, 2022, **24**, 854–862.
27 S. Hayashi, T. Koizumi and N. Kamiya, *ChemPlusChem*, 2019, **84**, 247–251.

28 E. Cho, J. Choi, S. Jo, D. H. Park, Y. K. Hong, D. Kim and T. S. Lee, *ChemPlusChem*, 2019, **84**, 1130–1134.
29 M. Shimizu, R. Shigitani, T. Kinoshita and H. Sakaguchi, *Chem.–Asian J.*, 2019, **14**, 1792–1800.
30 R. Huang, B. Tang, K. Ye, C. Wang and H. Zhang, *Adv. Opt. Mater.*, 2019, **7**, 1900927.
31 S. D. Ohmura, T. Moriuchi and T. Hirao, *Tetrahedron Lett.*, 2010, **51**, 3190–3192.
32 H. Liu, S. Yan, R. Huang, Z. Gao, G. Wang, L. Ding and Y. Fang, *Chem.–Eur. J.*, 2019, **25**, 16732–16739.
33 H. Kim, Y. Kim and D. Lee, *Acc. Chem. Res.*, 2024, **57**, 140–152.
34 J. N. Zhang, H. Kang, N. Li, S. M. Zhou, H. M. Sun, S. W. Yin, N. Zhao and B. Z. Tang, *Chem. Sci.*, 2017, **8**, 577–582.
35 Z. Xiang, Z. Y. Wang, T. B. Ren, W. Xu, Y. P. Liu, X. X. Zhang, P. Wu, L. Yuan and X. B. Zhang, *Chem. Commun.*, 2019, **55**, 11462–11465.
36 H. Kim, W. Park, Y. Kim, M. Filatov, C. H. Choi and D. Lee, *Nat. Commun.*, 2021, **12**, 5409.
37 T. Raghava, A. Chattopadhyay, S. Banerjee and N. Sarkar, *Org. Biomol. Chem.*, 2024, **22**, 364–373.
38 P. Takacsova, M. Kudlickova Peskova, P. Svec, Z. Heger and V. Pekarik, *Analyst*, 2023, **148**, 2058–2063.
39 T. Beppu, S. Kawata, N. Aizawa, Y. J. Pu, Y. Abe, Y. Ohba and H. Katagiri, *ChemPlusChem*, 2014, **79**, 536–545.
40 J. Kim, J. H. Oh and D. Kim, *Org. Biomol. Chem.*, 2021, **19**, 933–946.
41 M. Shimizu, *Chem. Rec.*, 2021, **21**, 1489–1505.
42 R. Zhou, Y. Cui, J. Dai, C. Wang, X. Liang, X. Yan, F. Liu, X. Liu, P. Sun, H. Zhang, Y. Wang and G. Lu, *Adv. Opt. Mater.*, 2020, **8**, 1902123.
43 A. Markovic, L. Buschbeck, T. Kluner, J. Christoffers and G. Wittstock, *ChemistryOpen*, 2019, **8**, 1176–1182.
44 Z. Bao, Y. Yang, X. Wu, Y. Ni, H. Zhou, Z. Zheng and B. Z. Tang, *Adv. Funct. Mater.*, 2024, **34**, 2403954.
45 D. Kim, S. Lee, H. Kim, J. Y. Kim, Y. Kim, Y. Kim, M. H. Park, D. Kim, J. Kwak, D. Kim and M. Kim, *Dyes Pigm.*, 2025, **233**, 112523.
46 J. H. Jin, J. M. An, D. Kim, S. Lee, M. Kim and D. Kim, *Dyes Pigm.*, 2024, **221**, 111811.
47 H. Kim, D. Kim, J. Y. Kim, S. Lee, W.-G. Yang, D. Kim, K. T. Kim, D. Kim, M. H. Park and M. Kim, *Synthesis*, 2024, **56**, 3859–3869.
48 J. H. Jin, D. Kim, J. Kang, S. Lee, J. M. An, M. Kim and D. Kim, *Bull. Korean Chem. Soc.*, 2024, **45**, 451–455.
49 C. Hansch, A. Leo and R. W. Taft, *Chem. Rev.*, 1991, **91**, 165–195.
50 H. C. Brown and Y. Okamoto, *J. Am. Chem. Soc.*, 1957, **79**, 1913–1917.
51 D. Kim, J. Y. Kim, H. Kim, E. Jeong, M. Lee, D. Kim, J. Kim, M. H. Park and M. Kim, *Chem. Commun.*, 2024, **60**, 14956–14959.
52 P. Xu, Q. Qiu, X. Ye, M. Wei, W. Xi, H. Feng and Z. Qian, *Chem. Commun.*, 2019, **55**, 14938–14941.
53 D. Dhingra, Bhawna, A. Pandey and S. Pandey, *J. Phys. Chem. B*, 2020, **124**, 4164–4173.
54 M. C. Chen, D. G. Chen and P. T. Chou, *ChemPlusChem*, 2021, **86**, 11–27.
55 M. J. Frisch, G. W. Trucks, H. B. Schlegel, G. E. Scuseria, M. A. Robb, J. R. Cheeseman, G. Scalmani, V. Barone, G. A. Petersson, H. Nakatsuji, X. Li, M. Caricato, A. V. Marenich, J. Bloino, B. G. Janesko, R. Gomperts, B. Mennucci, H. P. Hratchian, J. V. Ortiz, A. F. Izmaylov, J. L. Sonnenberg, D. Williams-Young, F. Ding, F. Lipparini, F. Egidi, J. Goings, B. Peng, A. Petrone, T. Henderson, D. Ranasinghe, V. G. Zakrzewski, J. Gao, N. Rega, G. Zheng, W. Liang, M. Hada, M. Ehara, K. Toyota, R. Fukuda, J. Hasegawa, M. Ishida, T. Nakajima, Y. Honda, O. Kitao, H. Nakai, T. Vreven, K. Throssell, J. A. Montgomery Jr, J. E. Peralta, F. Ogliaro, M. J. Bearpark, J. J. Heyd, E. N. Brothers, K. N. Kudin, V. N. Staroverov, T. A. Keith, R. Kobayashi, J. Normand, K. Raghavachari, A. P. Rendell, J. C. Burant, S. S. Iyengar, J. Tomasi, M. Cossi, J. M. Millam, M. Klene, C. Adamo, R. Cammi, J. W. Ochterski, R. L. Martin, K. Morokuma, O. Farkas, J. B. Foresman and D. J. Fox, *Gaussian 09, Revision A 02*, 2016.
56 S. Yang, Y. Yuan, X. Wang, Z. Hu and D. Guo, *J. Lumin.*, 2022, **242**, 118560.
57 K. Schniererova, H. Janekova, J. Joniak, M. Putala, P. Stacko and H. Stankovicova, *Chem.–Eur. J.*, 2024, **30**, e202400111.
58 H. Liu, S. Zhang, L. Ding and Y. Fang, *Chem. Commun.*, 2021, **57**, 4011–4014.
59 V. Gomes, N. Mateus, V. de Freitas and L. Cruz, *Photochem. Photobiol. Sci.*, 2021, **20**, 513–521.